Published OnlineFirst October 10, 2014; DOI: 10.1158/0008-5472.CAN-14-1212

Cancer Research

Densely Ionizing Radiation Acts via the Microenvironment to Promote Aggressive *Trp53*-Null Mammary Carcinomas

Irineu Illa-Bochaca[1], Haoxu Ouyang[1], Jonathan Tang[2], Christopher Sebastiano[3], Jian-Hua Mao[2], Sylvain V. Costes[2], Sandra Demaria[1,3], and Mary Helen Barcellos-Hoff[1]

Abstract

Densely ionizing radiation, which is present in the space radiation environment and used in radiation oncology, has potentially greater carcinogenic effect compared with sparsely ionizing radiation that is prevalent on earth. Here, we used a radiation chimera in which mice were exposed to densely ionizing 350 MeV/amu Si-particles, γ-radiation, or sham-irradiated and transplanted 3 days later with syngeneic *Trp53*-null mammary fragments. *Trp53*-null tumors arising in mice irradiated with Si-particles had a shorter median time to appearance and grew faster once detected compared with those in sham-irradiated or γ-irradiated mice. Tumors were further classified by markers keratin 8/18 (K18, *KRT18*), keratin 14 (K14, *KRT14*) and estrogen receptor (ER, *ESR1*), and expression profiling. Most tumors arising in sham-irradiated hosts were comprised of both K18- and K14-positive cells (K14/18) while those tumors arising in irradiated hosts were mostly K18. Keratin staining was significantly associated with ER status: K14/18 tumors were predominantly ER-positive, whereas K18 tumors were predominantly ER-negative. Genes differentially expressed in K18 tumors compared with K14/18 tumor were associated with ERBB2 and KRAS, metastasis, and loss of E-cadherin. Consistent with this, K18 tumors tended to grow faster and be more metastatic than K14/18 tumors, however, K18 tumors in particle-irradiated mice grew significantly larger and were more metastatic compared with sham-irradiated mice. An expression profile that distinguished K18 tumors arising in particle-irradiated mice compared with sham-irradiated mice was enriched in mammary stem cell, stroma, and Notch signaling genes. These data suggest that carcinogenic effects of densely ionizing radiation are mediated by the microenvironment, which elicits more aggressive tumors compared with similar tumors arising in sham-irradiated hosts. *Cancer Res; 74(23); 1–12. ©2014 AACR.*

Introduction

Ionizing radiation is one of a few demonstrable carcinogens of the human breast (1). Sparsely ionizing radiation is prevalent in the terrestrial environment as well as in medical uses. Densely ionizing radiation is a major component of the space radiation environment and is gaining traction for use in radiation oncology. Both radiation types evoke acute and persistent, short and long range effects (2–5), but experimental data from mouse models suggest that densely ionizing radiation has potentially greater carcinogenic effects compared with sparsely ionizing radiation (6, 7). Microscopic dose distribution is a major difference between sparsely and densely ionizing radiation (7). Densely ionizing radiation from charged particles delivers a high dose to a very small volume along the trajectory of the particle while sparsely ionizing radiation delivers an equivalent dose throughout the volume. One may compare similar absorbed dose but microscopic distribution is different and the biologic outcomes can be both quantitatively (e.g., cell kill, mutations) and qualitatively (e.g., gene expression, cell fate) different. Thorough understanding of the carcinogenic potential of densely ionizing radiation is important to assess the risk of space exploration and secondary malignant neoplasms following charged particle radiotherapy (8).

While DNA damage, misrepair, and mutations are thought to underlie the increase in cancer following radiation exposure, we and others have postulated that altered signaling between irradiated cells and tissues also contribute to its carcinogenic potential (9, 10). We have shown that both sparsely and densely ionizing radiation affects epithelial phenotype, including epithelial to mesenchymal transition, stromal remodeling, stem/progenitor self-renewal, and genomic instability in human cells and mouse tissues (reviewed in refs. 11 and 12). Many studies using oncogenic mouse models indicate that the stroma is highly involved in early malignancy (13) and that stroma composition and signaling is altered in human breast cancer (14), which support the idea of reciprocal evolution of the malignant cell and the tumor microenvironment (15). Less is known about how and when stroma contributes to carcinogenesis and how carcinogens like radiation might alter these processes.

[1]Department of Radiation Oncology, New York University School of Medicine, New York, New York. [2]Department of Pathology, New York University School of Medicine, New York, New York. [3]Life Sciences Division, Lawrence Berkeley National Laboratory, Berkeley, California.

Note: Supplementary data for this article are available at Cancer Research Online (http://cancerres.aacrjournals.org/).

Corresponding Author: Mary Helen Barcellos-Hoff, Department of Radiation Oncology, New York University School of Medicine, 450 E. 29th Street, New York, NY 10016. Phone: 212-263-3021; E-mail: mhbarcellos-hoff@nyumc.org

doi: 10.1158/0008-5472.CAN-14-1212

Published OnlineFirst October 10, 2014; DOI: 10.1158/0008-5472.CAN-14-1212

Also unknown is to what extent the carcinogenic potential as a function of radiation quality is mediated by differential effects on the irradiated microenvironment. To address this issue, we developed a radiation chimera mammary model to separate radiation-induced microenvironment from radiation-induced mammary epithelial DNA damage and potential mutation (16). The mammary gland is surgically cleared of endogenous epithelium, the mouse is irradiated, and the mammary fat pad subsequently orthotopically transplanted with unirradiated, nonmalignant epithelial cells that are primed for malignant transformation by *Trp53* deletion.

The *Trp53*-null mammary chimera is widely used as a syngeneic mouse model for breast carcinogenesis (17–21). Outgrowths from *Trp53*-null mammary epithelial transplants undergo broadly normal morphogenesis over the first 6 months and have a high rate of sporadic transformation and a slow rate of tumor formation. *Trp53*-null mammary epithelium progresses from ductal outgrowths to ductal carcinoma *in situ* to invasive breast carcinomas over the course of a year or more. The resulting cancers are diverse, similar to human tumors, including genomic instability, differential expression of estrogen receptor (ER) α and heterogeneous histology (19, 20, 22). This model has been used successfully to evaluate hormonal prevention strategies (23, 24), test chemopreventive agents (25–27), demonstrate the existence of cancer stem cells in mammary tumors (28, 29), and, in our hands, to study the mechanisms of ionizing radiation carcinogenesis.

In the radiation chimera model, in which mice are first irradiated before transplantation of *Trp53*-null tissue, the incidence of tumors arising in mice irradiated with 10 to 100 cGy of sparsely ionizing radiation increased compared with sham-irradiated mice (30). Moreover, tumors in irradiated mice also grow more rapidly and exhibit a distinct molecular signature. Notably, the molecular signature of tumors arising in irradiated mice compared with those arising in control mice is informative in human cancer. A host irradiation metaprofile consisting of 353 genes populating modules that represent stem cells, cell motility, macrophages, and autophagy discriminates between tumors arising in sham versus irradiated hosts (31). Human gene orthologs of this murine signature separate cancers arising in previously irradiated patients from sporadic cancers, which suggests that the carcinogenic effect of radiation mediated by the microenvironment is relevant to cancer risk in humans. When applied to sporadic human breast cancers, the irradiated host profile also clusters tumors according to intrinsic molecular subtype, is associated strongly with basal-like tumors, and specifically implicates TGFβ, a major signal in irradiated tissue, with immune and inflammatory modules in claudin-low human breast tumors. These bioinformatic analyses lend weight to the utility of the radiation chimera to provide new insight into both radiation-preceded and sporadic carcinogenic processes in humans.

The radiation-genetic chimera model demonstrates that radiation acts systemically on the host and tissue level to perpetuate and/or promote carcinogenic potential. Here, we used the radiation mammary chimera model to evaluate the effect of densely ionizing radiation. The biologic behavior and features of contemporaneous tumors arising from unirradiated *Trp53*-null mammary epithelium transplanted to sham-irradiated mice were compared with tumors arising in mice irradiated with 3 fluences of 350 MeV/amu Si particles (LET = 64 KeV/μm) or a reference dose of 100 cGy sparsely ionizing γ-radiation. Tumors arising in mice exposed to densely ionizing radiation grew significantly faster, were more likely to metastasize, and could be genomically separated from tumors with the same markers arising in sham-irradiated mice. These data suggest that the effects of densely ionizing radiation mediated by the microenvironment are more effective than sparsely ionizing radiation in eliciting aggressive tumors.

Materials and Methods

Animals

All animal experiments were performed at New York University School of Medicine (New York, NY) with institutional review and approval. BALB/c mice were purchased from Jackson Laboratory (Bar Harbor, Maine) and housed 4 per cage, fed with Lab Diet 5008 chow and water *ad libidum*. *Trp53*-null BALB/c mice were bred in-house under similar conditions. For transplantation experiments, the epithelial rudiments in inguinal glands of 3-week-old wild-type mice were surgically removed at the New York University. The mice were housed at New York University until they were transported to Brookhaven National Laboratory (Upton, New York) at 8 to 9 weeks of age. After acclimation, groups of mice were whole body irradiated with institutional approval at 10 weeks of age with 100 cGy γ-radiation using a 5600 curie (207 TBq) ^{137}Cs source or exposed to 3 fluences of 350 MeV/amu Si ions (64 KeV/μm) equivalent to 1, 3, or 5 particles/10 μm^2 (average dose 11, 30, and 81 cGy) delivered at the NASA Space Radiation Laboratory of Brookhaven National Laboratory. Doses were chosen in accordance with NASA investigational guidance for relevance to space radiation environment. All cohorts were contemporaneous. Three days after irradiation, the cleared mammary glands of host mice were transplanted with approximately 1 mm^3 fragment of nonirradiated *Trp53*-null mammary gland tissue that had been rapidly thawed from cryogenically preserved fragments of inguinal glands pooled from three or more, 8- to 10-week-old *Trp53*-null BALB/c female donor mice.

Mice were quarantined for 6 weeks upon return to the New York University and thereafter monitored by palpation 2 to 3 times per week for 600 days. Once a palpable tumor was detected, it was measured twice weekly using calipers until reaching 1 cm^3, at which point the first tumor was resected using survival surgery. Tumors were divided and frozen in liquid nitrogen for RNA extraction, embedded in optimum cutting temperature compound, or formalin-fixed followed by paraffin embedding. The mouse was further observed until the resected tumor recurred, at which point the mouse was euthanized, or until the contralateral fat pad developed a tumor, which was monitored as above. A gross necroscopy was performed upon termination. If no tumor developed by experiment termination, then an inguinal gland wholemount was prepared to determine successful transplantation; mammary glands in which transplantation failed were censored.

Published OnlineFirst October 10, 2014; DOI: 10.1158/0008-5472.CAN-14-1212

An informative transplant was defined as that which had an epithelial outgrowth evident by tumor development or wholemount confirmation at experiment termination.

Immunohistochemistry

Sections were deparaffinized and rehydrated before antigen unmasking according to manufacturer instructions (Vector Laboratories, #H-3300), washed once with PBS and blocked with 0.5% casein/PBS for 1 hour at room temperature. Primary antibodies for ER (NCL-ER-6F11, Novocastra), CK8/18 (20R-CP004, Fitzgerald), and K14 (PRB-155P, Covance) diluted in Superblock Blocking Buffer (Pierce, #37515) were added to slides and refrigerated overnight. The slides were washed, followed by incubation with fluorochrome-conjugated secondary antibody, washed and counterstained with 4′,6-diamidino-2-phenylindole (DAPI, 2 μg/mL; Molecular Probes). Allred scoring was used to determine ER status of tumors (32). Staining was technically confirmed by simultaneous inclusion of a positive control of normal mammary gland. Histopathologic characteristics of the tumors were reviewed by two observers blinded to the experimental details of the mouse models. Mitotic rate was counted in 5 high-power fields (HPF) for each tumor. Tumors were classified by two pathologists (C. Sebastiano and S. Demaria).

Expression profiling

Total RNA quality and quantity from tumors was determined using Agilent 2100 Bioanalyzer and Nanodrop ND-1000. Affymetrix mouse Genechip 1.0 ST arrays were used according to the manufacturer's protocol. Gene expression data is archived on Gene Expression Omnibus (GEO) under accession number GSE56704. Background subtraction and normalization was performed using the Robust Multichip Average algorithm from the Bioconductor package oligo (33). No filter was used unless specified as a SD of 1.0 relative to the expression values of that gene across all samples. Differentially regulated gene lists for pathway analysis were identified by feature selection algorithm Pavlidis template matching (PTM; ref. 34) using a $P < 0.05$ and a 1.5- or 1.25-fold change criterion. Gene clustering was done by a Pearson correlation and array clustering was done by Spearman Rank correlation. Enriched gene sets or pathway and upstream regulators were identified through the use of ConceptGen, Gene Set Enrichment Analysis with MSigDB database v4.0 or Ingenuity Pathway Analysis (IPA; Ingenuity Systems).

Statistical analysis

Statistical analysis of experimental data was performed using Prism (GraphPad). Differences between treatment groups were determined using the χ^2 test, Mann–Whitney test or two-way ANOVA, as indicated in text. Time to tumor occurrence was plotted using Kaplan–Meier with significance determined by the log-rank test. Tumor growth rates for the first 30 days after palpation were fitted to an exponential curve, which were averaged for a treatment group. Differences were considered statistically significant at $P < 0.05$. Multidimensional scaling analysis and discriminant analysis was done in SPSS (SPSS, Inc., Chicago).

Results

Trp53-null mammary tumors develop more rapidly in mice exposed to densely ionizing radiation

The experimental sequence for this study is shown in Fig. 1A. Ten-week-old mice were irradiated with either 100 cGy of γ-radiation or with 350 MeV/amu Si particles to an average dose 11, 30, or 81 cGy, which represent particle fluences of 1, 3, or 8 particles, respectively, per 10 μm^2. Of 156 transplanted fat pads, 131 generated an outgrowth (84% transplant efficiency), and, of these, 81 (62%) generated a palpable tumor during the observation period of 600 days. The earliest tumors appeared around 200 days after transplantation. Tumor incidence at 600 days after transplantation (approximately 670 days of age) at experiment termination for sham, γ−irradiated, and all Si-particle doses combined was 63%, 54%, 66%, respectively. No significant difference in transplantation efficiency or mortality was observed for irradiated groups compared with sham.

The median time to tumor detection in mice irradiated with the lowest Si-fluence or γ-radiation was similar to that in sham-irradiated mice but decreased in a dose-dependent fashion for transplants in mice exposed to Si-irradiation. (Fig. 1B). Once palpable, the growth rate of individual *Trp53*-null tumors was highly variable (Fig. 1C–G). To permit comparison among groups, each growth curve within a treatment group was fitted as an exponential curve, which was used to extrapolate tumor size for a period representing the 30 day postdetection. The r values (>0.9) indicate that this is a reliable representation of the growth trajectory; therefore, tumor sizes for all tumors in a treatment group were averaged for every day of the 30 days, independent of when the tumor arose. The growth rate of tumors arising in irradiated mice was increased compared with those arising in sham-irradiated mice (Supplementary Fig. S1). The initial growth rate (i.e., first 30 days) of tumors arising in mice exposed to 81 cGy and 30 cGy Si-particles was significantly faster than tumors in sham-irradiated mice (Fig. 1H). The initial growth rate of tumors arising in hosts irradiated with 11 cGy Si-particles was comparable with that of tumors arising in mice irradiated with 100 cGy sparsely ionizing γ-rays, which was modestly increased compared with tumors in sham-irradiated hosts, as previously reported (30). The effect of host irradiation with either 100 cGy γ or 11 cGy Si-particles (∼1 particle/cell) on decreased median latency and increased tumor growth rate were comparable, indicating a relative biologic effectiveness of 10.

Trp53-null tumors are histologically and molecularly diverse (19, 20, 22). The features of tumors as function of host irradiation are summarized in Supplementary Table S1. Most tumors were adenocarcinomas and the remaining were metaplastic carcinomas. The distribution of tumor histology was not affected by host irradiation, except in the high dose Si-particle–irradiated mice, in which there were more metaplastic carcinomas.

Approximately 70% of human breast cancers are positive for ER by immunostaining, which is a positive prognostic factor whereas the prognosis for ER-negative breast cancer is much poorer (35). Our prior studies show that irradiating hosts with either sparsely or densely ionizing radiation shifted the

Published OnlineFirst October 10, 2014; DOI: 10.1158/0008-5472.CAN-14-1212

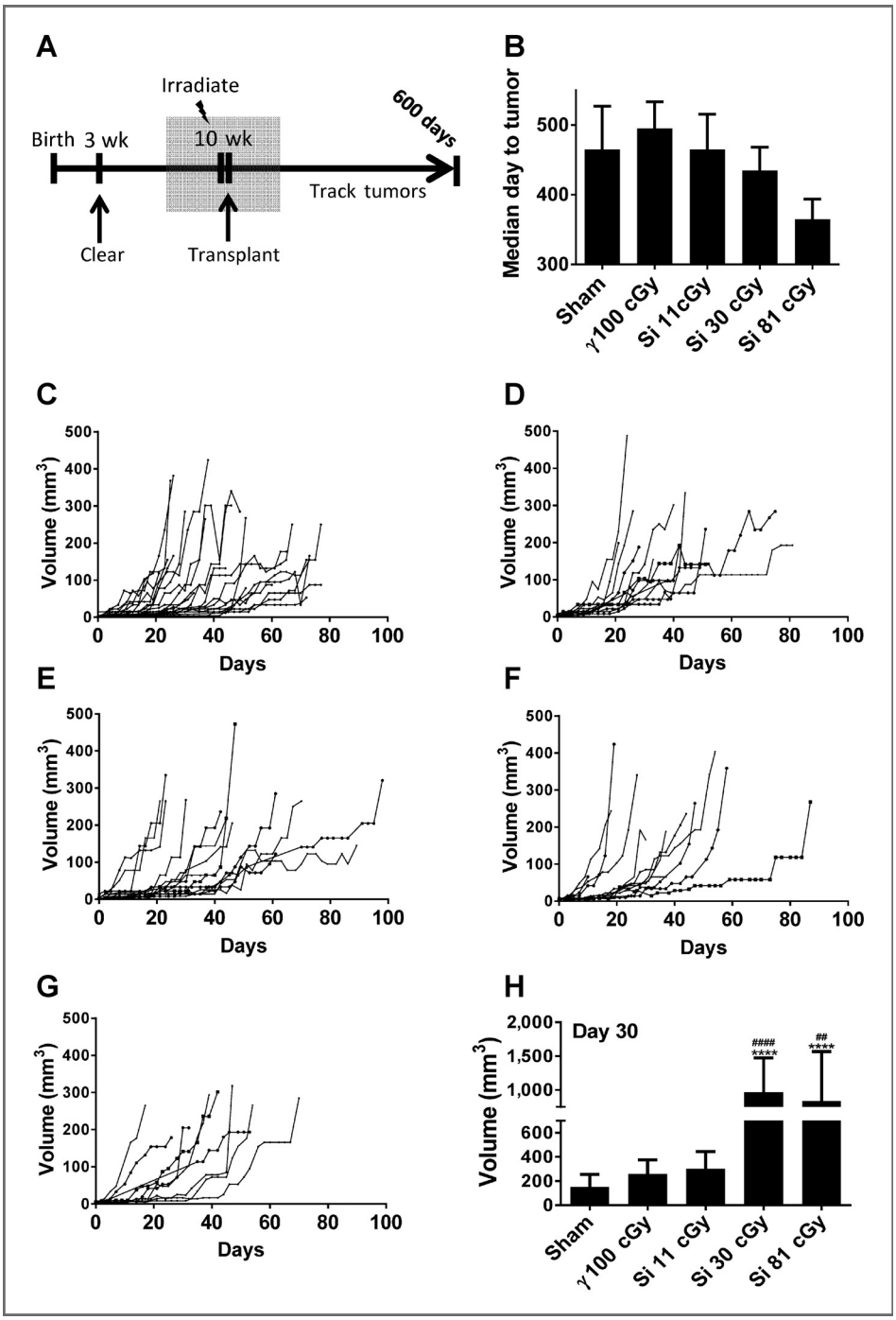

Figure 1. Host irradiation increases *Trp53*-null tumorigenesis. A, timeline of the host irradiation experiment. B, median day to tumor detection as a function of host. C–G, growth rates of individual tumors in sham-irradiated control mice ($n = 23$; C), or γ 100 cGy ($n = 12$; D), Si 11 cGy ($n = 14$; E), Si 30 cGy ($n = 12$; F), and Si 81 cGy ($n = 9$; G) irradiated hosts. H, tumor volume at day 30 generated from fitted tumor growth curves for each irradiation group. The calculated volume was averaged per treatment. Two-way ANOVA was performed to compare the tumor volume at each day between different irradiation groups. Sham, $n = 23$; γ 100 cGy, $n = 12$; Si 11 cGy, $n = 14$; Si 30 cGy, $n = 12$; Si 81 cGy, $n = 9$. ****, $P < 0.0001$, compared with the sham-irradiated group. ##, $P < 0.01$; ####, $P < 0.0001$, compared with γ 100 cGy or Si 11 cGy.

dominant tumor type from ER-positive to ER-negative (30, 36). Most (62%, $n = 15/24$) tumors arising in sham-irradiated mice were ER-positive, compared with 33% ($n = 4/12$) in γ-irradiated hosts and 43% ($n = 15/35$) in Si-irradiated (combined dose groups) hosts. Given this differential, we asked whether growth rate changed as a function of ER status. There was little difference between the growth rate ER-negative tumors and ER-positive tumors (Supplementary Fig. S2), which does not support ER status as a primary determinant of growth rate. However, ER-negative tumors arising in Si-particle–irradiated hosts grew significantly faster than those in either sparsely ionizing irradiated or sham-irradiated hosts. The gain in tumor volume in the initial 30 days of ER-negative tumors arising in Si-particle–irradiated hosts was more than 5-times (1,033 ± 541 mm^3, $n = 20$) that of tumors in sham-irradiated hosts (171 ± 95 mm^3, $n = 9$) or γ-irradiated hosts (150 ± 80 mm^3, $n = 8$), suggesting that host particle irradiation promotes more aggressive, ER-negative tumors.

Published OnlineFirst October 10, 2014; DOI: 10.1158/0008-5472.CAN-14-1212

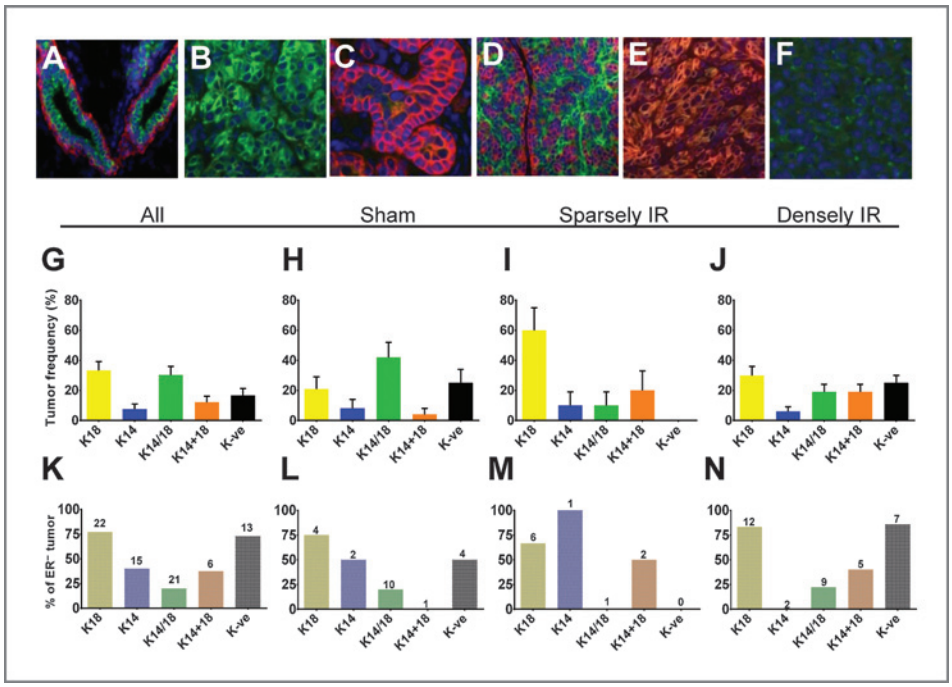

Figure 2. Host irradiation affects the distribution of *Trp53* null mammary carcinomas. A–F, dual immunostaining using K14 and K8/18 antibodies of normal mammary duct (A). The basal, myoeptithelial cell populations were stained positively for K14 (red) and the luminal, epithelial cells were positive for K18 (green). Nuclei were counterstained with DAPI (blue). B–F, keratin patterns found in *Trp53*-null mammary tumors ($n = 66$) were characterized as K18 type ($n = 22$, yellow; B), K14 ($n = 5$, blue; C), K14/18 type with cells positive either for K18 or K14 ($n = 20$, green; D), K14+18 type with K14 and K18 colocalized in the same cells ($n = 8$, orange; E), and K18 and K14-negative type ($n = 11$, black; F). G–J, frequency of different keratin tumor types in all mice ($n = 66$; G), sham-irradiated hosts ($n = 21$; H), γ-irradiated hosts (sparsely IR, $n = 10$; I), and Si-irradiated hosts (densely IR, $n = 35$; J). K–N, the frequency of ER-negative tumor as a function of keratin tumor type from all (K), or sham-irradiated (L), γ-irradiated (M), and Si-irradiated hosts (N) as above. The number of tumor in each keratin tumor type was indicated on top of each bar.

Tumor type is thought to be related to the cell of origin (reviewed in ref. 37). The murine mammary gland consists of two major cell types, basal myoepithelial cells that express keratin 14 (K14) and p63, and luminal cells that express keratin 8/18 (K18) and steroid hormone receptors, similar to those found in human breast (38). Dual immunofluorescence for K14 and K18 demonstrates these distinct cell types in normal mouse mammary epithelium (Fig. 2A). We then classified tumors using dual K14/K18 immunostaining. Five patterns of keratin reactivity were identified in tumors (Fig. 2B–F): predominantly (>80%) K14, predominantly K18, tumors composed of both K14 and K18 cells organized in a pseudoglandular pattern (designated K14/18), tumors in which at least 30% of cells were positive for both keratins simultaneously, and tumors negative for either.

The distribution of tumor keratin patterns was significantly different between hosts irradiated with sparsely ($n = 12$) or densely ($n = 35$) ionizing radiation compared with tumors arising in sham-irradiated hosts (Fig. 2G–J; $n = 24$). Most tumors that arose in sham-irradiated hosts were K14/18, whereas host irradiation with either radiation quality favored K18 tumors at the expense of K14/18 tumors (χ^2, $P < 0.05$).

Keratin staining was significantly associated with ER status (χ^2, $P < 0.001$). K14/18 tumors were predominantly ER-positive (16/20, 80%) and K18 tumors were predominantly ER-negative (17/22, 77%; Fig. 2K). Interestingly tumors that were negative for either keratin were frequently ER-negative and were absent from γ-irradiated mice and were more frequent in Si-irradiated hosts compared with sham-irradiated hosts (Fig. 2L–N). These data suggest that host Si irradiation primarily promotes specific ER-negative subtypes.

Although K18 tumors tended to grow faster than K14/18 tumors, host irradiation with either radiation type increased K18 tumor initial growth but Si particle host irradiation was significantly more effective than γ-radiation (Fig. 3A). Interestingly, K14/18 tumor growth was not increased in irradiated hosts compared with the sham-irradiated hosts (Fig. 3B). In support of a distinct biology of K18 tumors in irradiated hosts, the metastatic potential of K18 tumors was increased in irradiated hosts (Fig. 3C); again, this was not observed in mice with K14/18 tumors (Fig. 3D). These data suggested that particle irradiation both enriches for a particular tumor type and promotes its progression.

Given the complexity of tumor features, we then conducted multidimensional scaling analysis to determine how phenotypes associate with each other. Tumors arising in 11 cGy Si particle or 100 cGy γ-irradiated hosts were grouped close together with those arising in sham-irradiated mice based on ER status, lung tumor, necrosis and invasion, which was only weakly associated with keratin status (Fig. 4A). Latency, growth rate, and mitotic index were independent of this cluster and with each other. For tumors arising in mice irradiated with 30 or 81 cGy Si particles, nuclear grade was grouped with ER status, lung tumor, necrosis, and invasion, and again weakly

Published OnlineFirst October 10, 2014; DOI: 10.1158/0008-5472.CAN-14-1212

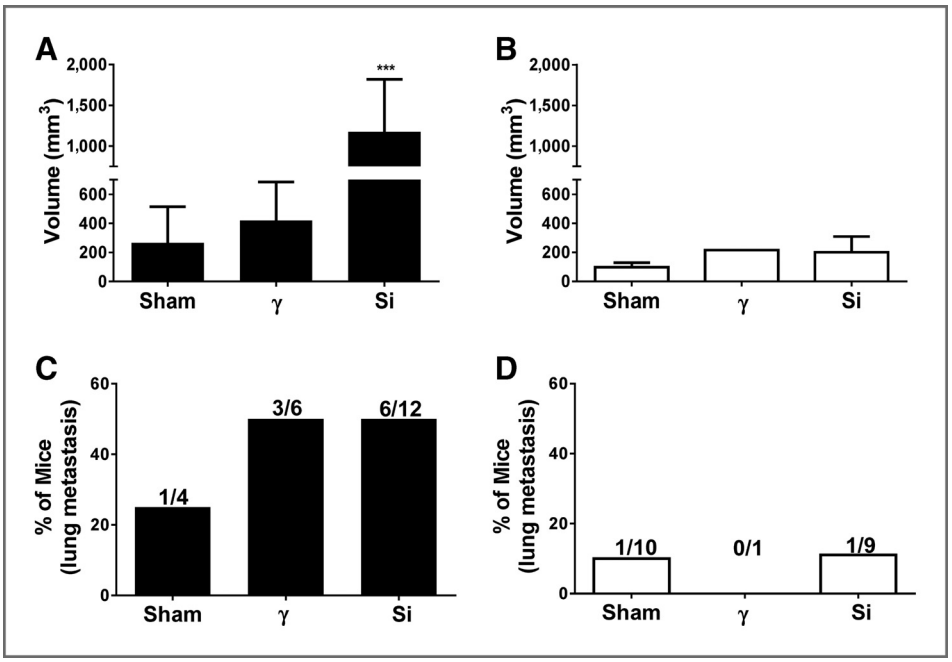

Figure 3. Host irradiation enhances tumor growth and lung metastasis of K18 but not K14/18 tumors. A and B, tumor volumes at day 30 for K18 (A) and K14/18 tumors (B) from sham-, γ-, or Si-irradiated mice. Two-way ANOVA was performed to compare the tumor volume at each day between different irradiated hosts. ***, $P < 0.001$, compared with the sham-irradiated group. C and D, observed frequency of lung metastasis from mice that previously developed a K18 (C) or K14/18 (D) mammary gland tumor. Only mice developed with unilateral mammary tumor were included. Number of mice with and without lung metastases is indicated on top of the bar.

associated with keratin type (Fig. 4B). However, consistent with their increased growth rate, mitotic rate and tumor growth rate were associated with each other in this group. Interestingly, latency was not associated with any feature in any group. Discriminant analysis also indicated that tumors arising in 11 cGy Si, 100 cGy, and sham-irradiated hosts were more similar than those arising 30 and 81 cGy Si-particle–irradiated hosts (Fig. 4C).

Expression signatures of K18 versus K14/18 tumors

Given the shift in tumor subtype elicited in the context of the Si-particle–irradiated host, we used Affymetrix mouse Genechip 1.0 ST arrays to profile 45 tumors and conducted unsupervised hierarchical clustering of genes with variability greater than 1 SD across samples. We noted that almost all K14/18 (11/14) and K18 (11/12) tumors were clustered in one of two major dendrogram arms (Supplementary Fig. S3). We then compared the profiles of these keratin subtype tumors arising in sham-irradiated mice. PTM identified 330 upregulated genes and 367 downregulated genes in K18 compared with K14/18 tumors (Fig. 5A). The human orthologs of these gene lists (278/330 and 295/367) were classified using ConceptGen and gene set enrichment analysis (GSEA). Among genes decreased in K18 compared with K14/18 tumors are significantly enrichment of genes suppressed in metastasis lesion ($P = 1.20 \times 10^{-35}$) or by loss of E-cadherin ($P = 1.25 \times 10^{-24}$). In terms of function, those genes, such as *Col17a1*, *Lama3*, and *Cdh3*, have been shown to be involved in cell adhesion and cell–cell junction (Fig. 5A). Consistent with this, the frequency of lung metastasis was increased in mice bearing K18 tumors compared with K14/18 tumors (Fig. 3C and D).

The K18 tumor profile was also enriched in genes that are present in the luminal B breast cancer signature ($P = 0.005$), whereas genes highly expressed in basal breast cancer were under expressed ($P = 6.70 \times 10^{-4}$). Classic basal keratins Krt5 and Krt14 were under expressed in K18 tumors. Genes represented in the MaSC signature, defined by Lim and colleagues (39), were enriched in both tumors but, interestingly, their expression was in the opposite direction; that is, genes highly expressed in MaSC were suppressed in K18 tumors and vice versa (Supplementary Fig. S4). Genes increased in K18 tumors were enriched in genes upregulated with activation of ERBB2 ($P = 2.56 \times 10^{-36}$) and KRAS ($P = 5.46 \times 10^{-12}$). Activation of these genes is strongly associated with aggressive tumors (28, 29). Moreover, several components of Wnt signaling were overexpressed in K18 tumors (Fig. 5A), which may contribute to the aggressiveness of K18 tumors. Consistent with all these molecular features, tumor growth rate of K18 tumors in sham-irradiated mice tended to grow slightly faster than K14/18 tumors but this was not significantly different, possibly due to the small numbers of tumors in sham-irradiated mice.

Together, these data suggested that K18 and K14/18 tumors may be murine correlates of intrinsic subtypes in human tumors. To test this idea, we evaluated how the biology represented by the K18 versus K14/18 profile relates to human breast cancer. We used a database that consists of 1,608 breast cancers classified into five intrinsic subtypes using PAM50 (40). The human orthologs of the K18 versus K14/18 profile clustered breast cancer into two major groups (Fig. 5B). One group contained many normal-like tumors and luminal tumors but almost no basal-like tumors. The other major group had three subgroups. Group 2A mainly consists of basal-like and normal-like tumors whereas group 2B is filled with basal-like tumor predominately. Group 2C contains a block of luminal tumors and two blocks of mixed tumors. Thus, the biology of *Trp53*-null tumors with specific

Published OnlineFirst October 10, 2014; DOI: 10.1158/0008-5472.CAN-14-1212

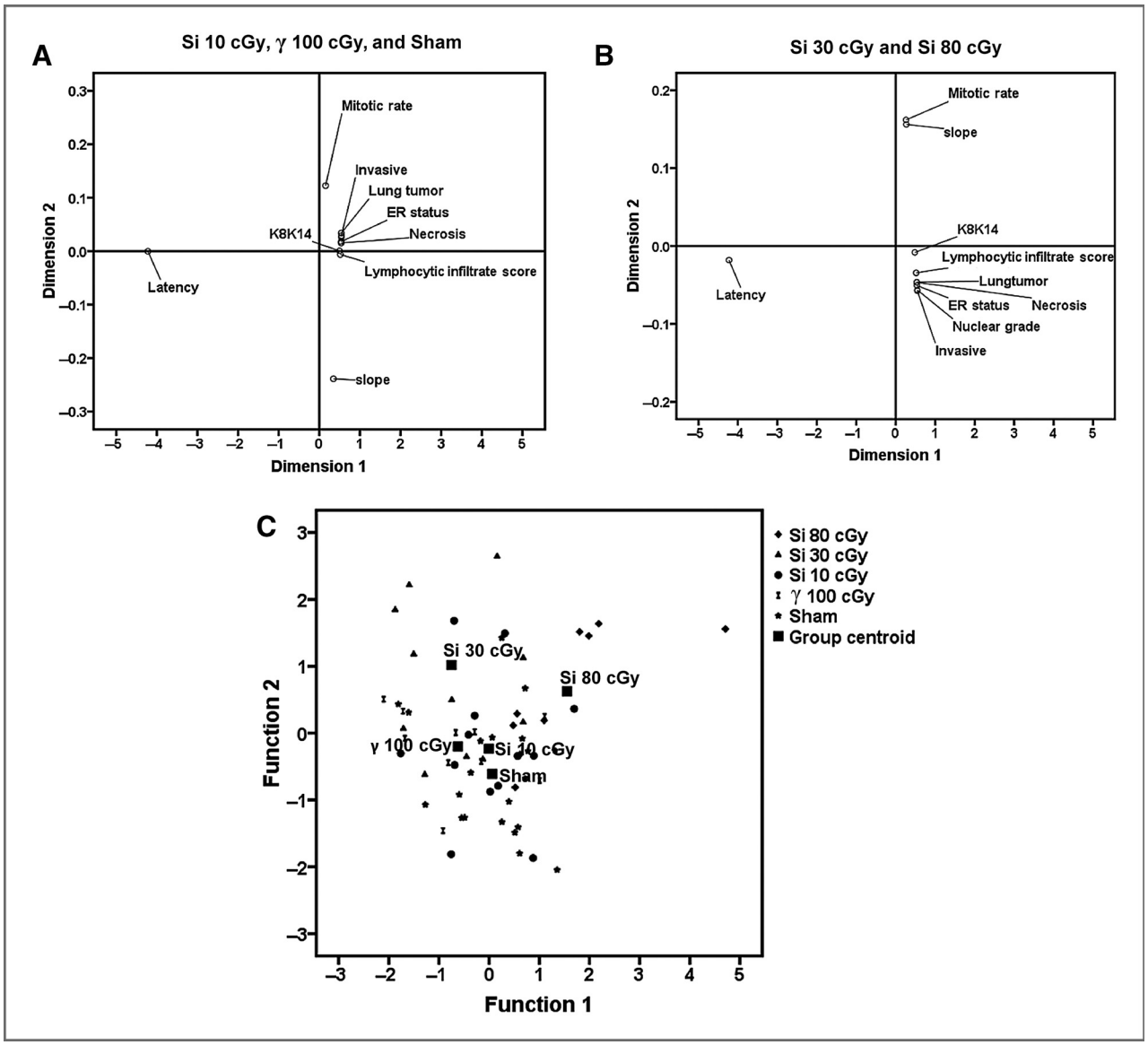

Figure 4. Association between tumor features and radiation dose and quality. Multidimensional scaling analysis was used to investigate how different tumor phenotypes are associated with each other in different radiation treated group. A, tumor features were similarly associated among tumors arising in mice irradiated with Si 11 cGy or γ 100 cGy or sham-irradiated. B, a similar pattern of association was evident among tumor features in Si 30 cGy- and Si 81 cGy–treated groups. C, discriminant analysis was used to find whether these phenotypes can distinguish one radiation-treated group from others. The group centroid, which averages the functional values, shows that tumor phenotypes discriminate between tumors arising in irradiated mice.

keratin markers has discriminant power in classifying human breast cancer.

Expression profiles of tumors arising in Si-particle–irradiated hosts

We next conducted a PTM analysis ($P < 0.05$, FC > 1.25) of tumors arising in Si-irradiated hosts compared with sham-irradiated hosts as a function of ER status (Fig. 5C and D). Host irradiation exerts more robust effects on gene expression profile in ER-negative than ER-positive tumors in that 1,078 genes were differentially expressed in ER-negative tumors while only 154 genes were ER-positive tumors. The MaSC signature was highly enriched in ER-negative tumors arising in irradiated hosts ($P = 1.6 \times 10^{-4}$) but not in ER-positive tumors ($P = 3.2 \times 10^{-1}$).

Given the more aggressive behavior of K18 tumors in Si-irradiated hosts, we hypothesized that they would be genomically distinct. To explore the effect of host irradiation on specific tumor types, we used PTM to generate Si-irradiated host profiles for K18 tumors (K18-IHPsi) and K14/18 tumors (K14/18-IHPsi). We were unable to make a comparison to similar tumors from γ-irradiated hosts because of the small number of contemporaneous tumors. We used PTM to identify 295 upregulated genes (corresponding to 241 human orthologs) and 162 downregulated

Published OnlineFirst October 10, 2014; DOI: 10.1158/0008-5472.CAN-14-1212

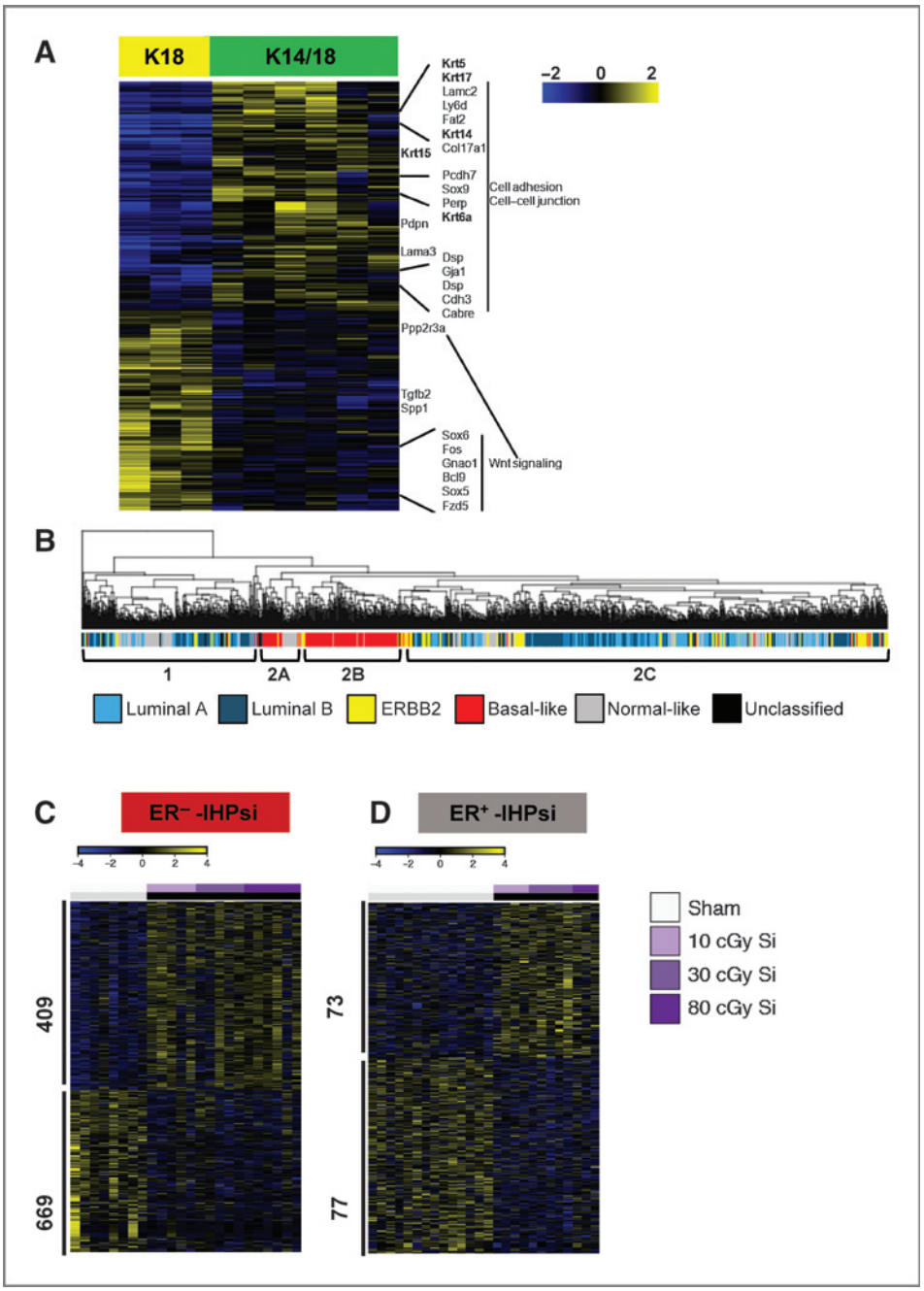

Figure 5. Comparison of features of K18 versus K14/18 tumors. A, heatmap of K18 versus K14/18 profile. Differentially expressed genes between K18 and K14/18 were identified by PTM. Important genes, biologic process, and pathway are marked on the heatmap. Genes in bold were keratins differentially expressed between K18 and K14/18 tumors. B, unsupervised clustering of 1,608 human breast cancers using 573 human orthologs of the murine genes from the K18 versus K14/18 profile. Tumors were segregated into four subgroups, some of which contained a predominant molecular subtype (luminal A, light blue; luminal B, dark blue; ERBB2, yellow; basal-like, red; normal-like, grey; and unclassified, black). C and D, gene expression profile from ER-negative tumors (ER-neg-IHPsi) and ER-positive tumors (ER-pos-IHPsi) arising from Si-irradiated host were identified using PTM ($P < 0.05$, FC > 1.25). The 1,078 genes (669 were upregulated and 409 were downregulated) were differentially expressed in ER(−) tumors upon host irradiation. Seventy-seven genes were upregulated, whereas 73 were downregulated in ER(+) tumors after host irradiation.

genes (corresponding to 111 human orthologs) in K18 tumors arising in Si-irradiated host compared with tumors arising in sham-irradiated. In contrast, gene expression profiles of K14/18 tumors arising in Si-irradiated hosts were more similar to those arising in sham-irradiated mice. Only 160 genes were differentially regulated: 106 upregulated genes (corresponding to 94 human orthologs) and 54 downregulated genes (corresponding to 46 human orthologs). Only 9 genes were common between K18-IHPsi and K14/18-IHPsi, suggesting that host irradiation affected each tumor type differently.

IPA analysis revealed that different networks were affected by host irradiation in each tumor type. Cell-cycle pathways, including estrogen-mediated S-phase entry and G_1–S checkpoint regulation, were enriched in K18-IHPsi (Fig. 6A). Expression of *CCND1*, *E2F3*, and *E2F4* were elevated by 65%, 70%, and 90% respectively in K18 tumors arising from Si-irradiated hosts compared with sham-irradiated hosts, consistent with their significantly faster growth rate. Epithelial–mesenchymal transition pathways were significantly associated with K18-IHPsi (Fig. 6A). Predictive analysis of the upstream regulators in K18-IHPsi signature include genes implicated in proinflammatory immune response (*TNF*, *IL4*, and *IL6*), TGFβ pathway members and targets important for microenvironment and angiogenesis (*TGM2*, *FGF2*, *SMAD3*, *TGFβ1*, *VEGFA*), and

Published OnlineFirst October 10, 2014; DOI: 10.1158/0008-5472.CAN-14-1212

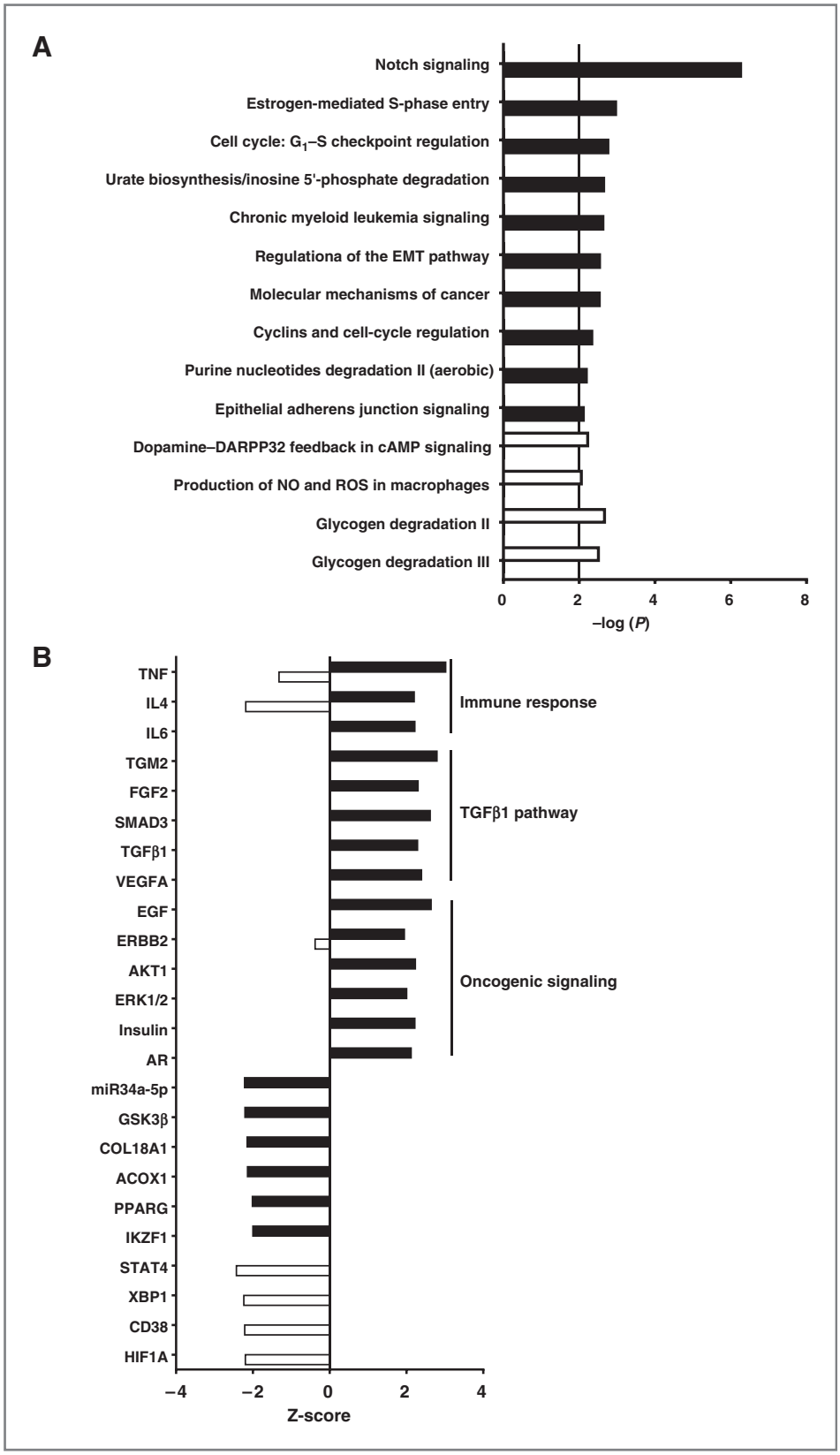

Figure 6. Host irradiation promotes distinct expression profiles in K18 and K14/18 tumors. A, canonical pathways identified by IPA. The *P* value $\leq$ 0.01 or $-$log10 (*P* value) $\geq$2 suggest that there is a significant overlap between a set of genes in K18 IHPsi (black bar) or K14/18-IHPsi (open bar) and genes implicated in a particular pathway. B, upstream regulators identified by IPA. The upstream regulators that are expected to be increased or decreased according to the gene expression changes in K18-IHPsi (black bar) or K14/18-IHPsi (open bar) were identified using the IPA *z*-score algorithm. A positive or negative *z*-score value indicates that upstream regulator is predicted to be activated or inhibited by host irradiation in specific tumor type. Only upstream regulators with a *z*-score $\geq$2 or ≤ -2 were considered as significant.

Published OnlineFirst October 10, 2014; DOI: 10.1158/0008-5472.CAN-14-1212

well-known genes in the canonical oncogenic signaling (*EGF*, *ERBB2*, *AKT1*, *ERK1/2*; Fig. 6B). Notably, none of these pathways or upstream regulators was activated in K14/18-IHPsi (Fig. 6A and B).

Aberrant Notch activation is associated with poor outcomes in human breast cancer, possibly via its role in regulating MaSC and luminal progenitor cells (41, 42). As found previously in irradiated tissues and tumors arising in γ-irradiated mice (30, 31), Notch signaling was activated in K18-IHPsi (Fig. 6A). In addition, both ConceptGen analysis and GSEA of K18-IHPsi found enrichment of genes highly expressed in the MaSC ($P = 2.33 \times 10^{-7}$) and stroma cell signatures ($P = 1.33 \times 10^{-7}$) defined by Lim and colleagues (39). Genes decreased in MaSC signature were also decreased in K18-IHPsi ($P = 7 \times 10^{-5}$), consistent with their ER-negative status, and likely reflecting the MaSC as cell of origin (36). This signature was not evident in K14/18-IHPsi, suggesting that host irradiation has tumor-specific engagement (Supplementary Fig. S5). Together, these data demonstrate that *Trp53* tumors classified by ER and keratin protein expression are genomically distinct, but K18-positive, ER-negative tumors that arise in mice irradiated with Si particles are distinct from similar tumors that arose in sham-irradiated mice.

Discussion

Here, we show that densely ionizing radiation acts through the microenvironment to promote more aggressive behavior and characteristics of *Trp53*-null mammary carcinomas. The galactic cosmic radiation environment is unlike any on earth because it includes charged particle species from protons through uranium at varying energies of up to tens of GeV/amu (7). Estimating the cancer risk of densely ionizing radiation for humans is difficult in the absence of exposed populations comparable with those exposed to sparsely ionizing radiation by accidents, medical need, and atomic bomb detonation. The limited experimental data to date indicate that densely ionizing particles are more effective in inducing cancer than sparsely ionizing radiation. The unique pattern of energy deposition incurred by particle traversal is considered to be the basis for differences in the biologic effects of the galactic cosmic radiation on astronauts (6). Comparison of sparsely and densely ionizing radiation indicates that greater relative biologic effectiveness of densely ionizing radiation for many biologic endpoints. However, some biologic effects are not observed following sparsely ionizing radiation (43) and some radiation effects, like genomic instability, do not show classic dose responses (44).

Comparison of tumors arising in contemporaneous hosts that were γ-irradiated (100 cGy) to tumors arising in mice exposed to graded fluences of Si particles suggest that densely ionizing radiation had greater biologic effectiveness for two endpoints: median time to tumor and growth rate. Both accelerated tumor appearance and increased growth rate also show some Si particle fluence dependence, though it is difficult to estimate the magnitude without more complete dose response data. The effect of host irradiation with either 100 cGy γ or 11 cGy Si particles (~1 particle/cell) on median latency and tumor growth rate were comparable, indicating relative biologic effectiveness of 10. These data may be further complicated by interaction of factors, as evident in the greater acceleration of ER-negative tumors arising in Si-particle–irradiated hosts compared with γ-irradiated (Supplementary Fig. S2).

We attempted to determine whether distinct tumor types underlie the increased growth rate of tumors arising in Si particle–irradiated hosts using marker classification. Addition of basal and luminal cell keratins revealed a complex pattern of K18 and K14 expression. Notably, most ER-negative tumors were K18-positive and were increased in irradiated hosts. Unsupervised clustering of expression profiling suggested that keratin status was differentially distributed between the two major dendrogram arms. Direct comparison of K18 versus K14/18 tumors demonstrated that they are genomically distinct. The expression profile that distinguished the K18 from K14/18 was enriched in genes lost when E-cadherin is downregulated and decreased in metastatic tumors. Consistent with these programs, mice with K18 tumors were more likely to have lung metastases than those with K14/18 tumors. K18 tumor growth rate was not significantly greater than that of K14/18 tumors in sham-irradiated mice, but K18 tumor growth rate was significantly increased in irradiated hosts while that of K14/18 tumors was not. Thus, we concluded that tumors arising in Si-irradiated mice are enriched for ER-negative, K18-positive tumors, which are intrinsically classified as more aggressive than ER-positive tumors, but there is an additional effect from the irradiated host that specifically affects these behaviors.

Cell type–based ontological and high-throughput molecular -omics are complimentary approaches to characterizing cancers (38). In a previous study, we found that gene expression profiles from γ- or Si-irradiated mammary gland tissue were comparable in terms of enriching for MaSC signature and implicating NOTCH, TGFβ, WNT pathways as upstream regulators (23) up to 12 weeks postirradiation. Tumors arising in hosts irradiated with low doses of sparsely ionizing radiation show a distinct gene expression profile, even though tumors occur many months postirradiation, and even when segregated by ER status (30, 31). Because of insufficient number of contemporaneous tumors from γ-irradiated host, we were not able to compare the quality difference at the molecular level or control for tumor marker status. However, we compared the IHPsi (all doses) with our published 323 gene signature (323-IHC) derived from tumors arising in hosts exposed to sparsely ionizing radiation (31). Although stem cell signaling was invoked in both 323-IHC and IHPsi, there is no overlap between the 323-IHC gene list and IHPsi, suggestive of a potential quality effect. In contrast, both K18-IHPsi and 323-IHC gene lists are enriched in TGFβ pathway, Notch signaling, and MaSC signatures. Again, the genes in each pathway do not overlap between the K18-IHPsi and 323-IHC lists. It may be that the different platforms used in these studies compromises the comparison; future studies will need to either use the same platforms or convert data between platforms.

Determining the relative carcinogenic contribution of radiation-targeted effects (e.g., genetic sequence) versus nontargeted effects (e.g., cell signaling) is important to understanding

Published OnlineFirst October 10, 2014; DOI: 10.1158/0008-5472.CAN-14-1212

cancer susceptibility. Radiation-induced DNA damage is broadly considered to be the primary mechanism determining its carcinogenic potential (45). There has been little change in this view of the biology underlying cancer risk in irradiated populations despite growing evidence that radiation affects systemic and cellular signaling in a complex and persistent fashion (9, 10, 46, 47). One of the main differences between these targeted and nontargeted response is the shape of the dose response. Signaling-mediated biology often shows switch-like dose dependence, as is seen in cells primed by radiation to undergo epithelial–mesenchymal transition (48). The tendency toward a saturation dose response would likely be more evident with more comprehensive dose/fluence response data for both densely and sparsely ionizing radiation.

Together, the data from this study support the idea that response of the host and microenvironment to radiation exposure significantly contribute to the carcinogenic process. Some endpoints (i.e., median latency, growth rate) suggest that densely ionizing radiation is more effective than sparsely ionizing radiation in stimulating progression. This possibility is likely to be of more immediate concern for predicting risk of second neoplasms following charged particle radiotherapy (8). Given that densely ionizing radiation acts through the microenvironment to increase tumor aggressiveness, it will be important to incorporate host determinants of cancer into risk modeling of radiation exposures in space and on earth.

Disclosure of Potential Conflicts of Interest

No potential conflicts of interest were disclosed.

Authors' Contributions

Conception and design: M.H. Barcellos-Hoff
Development of methodology: I. Illa-Bochaca
Acquisition of data (provided animals, acquired and managed patients, provided facilities, etc.): I. Illa-Bochaca, J. Tang, C. Sebastiano, J.-H. Mao, S. Demaria
Analysis and interpretation of data (e.g., statistical analysis, biostatistics, computational analysis): I. Illa-Bochaca, H. Ouyang, J. Tang, C. Sebastiano, J.-H. Mao, S.V. Costes, M.H. Barcellos-Hoff
Writing, review, and/or revision of the manuscript: I. Illa-Bochaca, H. Ouyang, J. Tang, J.-H. Mao, S. Demaria, M.H. Barcellos-Hoff
Administrative, technical, or material support (i.e., reporting or organizing data, constructing databases): I. Illa-Bochaca, S.V. Costes, M.H. Barcellos-Hoff
Study supervision: S.V. Costes, M.H. Barcellos-Hoff

Acknowledgments

The authors thank William Chou and Derek Francis for expert assistance.

Grant Support

This research was supported by NASA Specialized Center for Research in Radiation Health Effects, NNX09AM52G at the New York University School of Medicine.

The costs of publication of this article were defrayed in part by the payment of page charges. This article must therefore be hereby marked *advertisement* in accordance with 18 U.S.C. Section 1734 solely to indicate this fact.

Received April 24, 2014; revised August 15, 2014; accepted August 19, 2014; published OnlineFirst October 10, 2014.

References

1. Land CE, Boice JD, Shore RE, Norman JE, Tokunaga M. Breast cancer risk from low-dose exposures to ionizing radiation: results of parallel analysis of three exposed populations of women. J Natl Cancer Inst 1980;65:353–76.
2. Kaplan HS, Hirsch BB, Brown MB. Indirect induction of lymphomas in irradiated mice: IV. Genetic evidence of the origin of the tumor cells from the thymic grafts. Cancer Res 1956;16:434–6.
3. Barcellos-Hoff MH, Derynck R, Tsang ML-S, Weatherbee JA. Transforming growth factor-b activation in irradiated murine mammary gland. J Clin Invest 1994;93:892–9.
4. Amundson SA, Do KT, Fornace AJJ. Induction of stress genes by low doses of gamma rays. Radiat Res 1999;152:225–31.
5. Mancuso M, Pasquali E, Leonardi S, Tanori M, Rebessi S, Di Majo V, et al. Oncogenic bystander radiation effects in Patched heterozygous mouse cerebellum. Proc Natl Acad Sci U S A 2008;105:12445–50.
6. Blakely EA, Chang PY. Biology of charged particles. Cancer J 2009;15:271.
7. Durante M, Cucinotta FA. Heavy ion carcinogenesis and human space exploration. Nat Rev Cancer 2008;8:465–72.
8. Loeffler JS, Durante M. Charged particle therapy–optimization, challenges and future directions. Nat Rev Clin Oncol 2013;10:411–24.
9. Tubiana M. Dose-effect relationships and estimation of the carcinogenic effect of low doses of ionizing radiation: the joint report of the Académie des Sciences (Paris) and of the Nationale de Médecine. Int J Radiat Oncol Biol Phys 2005;63:317–9.
10. Barcellos-Hoff MH, Adams C, Balmain A, Costes SV, Demaria S, Illa-Bochaca I, et al. Systems biology perspectives on the carcinogenic potential of radiation. J Radiat Res 2014;55:i145–i54.
11. Barcellos-Hoff MH, Nguyen DH. Radiation carcinogenesis in context: How do irradiated tissues become tumors? Health Phys 2009;97:446–57.
12. Nguyen DH, Bochaca II, Barcellos-Hoff MH. The biological impact of radiation exposure on breast cancer development. In:Russo J, editor. Breast cancer and the environment. New York, NY: Springer; 2010.
13. Mueller MM, Fusenig NE. Friends or foes–Bipolar effects of the tumor stroma in cancer. Nat Rev Cancer 2004;4:839–49.
14. Finak G, Bertos N, Pepin F, Sadekova S, Souleimanova M, Zhao H, et al. Stromal gene expression predicts clinical outcome in breast cancer. Nat Med 2008;14:518–27.
15. Barcellos-Hoff MH, Lyden D, Wang TC. The evolution of the cancer niche during multistage carcinogenesis. Nat Rev Cancer 2013;13:511–8.
16. Barcellos-Hoff MH, Ravani SA. Irradiated mammary gland stroma promotes the expression of tumorigenic potential by unirradiated epithelial cells. Cancer Res 2000;60:1254–60.
17. Murphy KL, Rosen JM. Mutant p53 and genomic instability in a transgenic mouse model of breast cancer [see comments]. Oncogene 2000;19:1045–51.
18. Kuperwasser C, Hurlbut GD, Kittrell FS, Dickinson ES, Laucirica R, Medina D, et al. Development of spontaneous mammary tumors in BALB/c p53 heterozygous mice. A model for Li-Fraumeni syndrome. Am J Pathol 2000;157:2151–9.
19. Medina D, Kittrell FS, Shepard A, Stephens LC, Jiang C, Lu J, et al. Biological and genetic properties of the p53 null preneoplastic mammary epithelium. FASEB J 2002;16:881–3.
20. Jerry DJ, Kittrell FS, Kuperwasser C, Laucirica R, Dickinson ES, Bonilla PJ, et al. A mammary-specific model demonstrates the role of the p53 tumor suppressor gene in tumor development. Oncogene 2000;19:1052–8.
21. Yan H, Blackburn AC, McLary SC, Tao L, Roberts AL, Xavier EA, et al. Pathways contributing to development of spontaneous mammary tumors in BALB/c-*Trp53*+/− mice. Am J Pathol 2010;176:1421–32.
22. Herschkowitz JI, Zhao W, Zhang M, Usary J, Murrow G, Edwards D, et al. Comparative oncogenomics identifies breast tumors enriched in functional tumor-initiating cells. Proc Natl Acad Sci U S A 2011;109:2778–83.

Published OnlineFirst October 10, 2014; DOI: 10.1158/0008-5472.CAN-14-1212

23. Rajkumar L, Kittrell F, Guzman R, Brown P, Nandi S, Medina D. Hormone-induced protection of mammary tumorigenesis in genetically engineered mouse models. Breast Cancer Res 2007;9:R12.
24. Dunphy K, Blackburn A, Yan H, O'Connell L, Jerry DJ. Estrogen and progesterone induce persistent increases in p53-dependent apoptosis and suppress mammary tumors in BALB/c-Trp53+/− mice. Breast Cancer Res 2008;10:R43.
25. Abba MC, Hu Y, Levy CC, Gaddis S, Kittrell FS, Hill J, et al. Identification of modulated genes by three classes of chemopreventive agents at preneoplastic stages in a p53-null mouse mammary tumor model. Cancer Prev Res 2009;2:175–84.
26. Medina D, Kittrell F, Hill J, Zhang Y, Hilsenbeck SG, Bissonette R, et al. Prevention of tumorigenesis in p53-null mammary epithelium by rexinoid bexarotene, tyrosine kinase inhibitor gefitinib, and celecoxib. Cancer Prev Res 2009;2:168–74.
27. Mazumdar A, Medina D, Kittrell FS, Zhang Y, Hill JL, Edwards DE, et al. The combination of tamoxifen and the rexinoid LG100268 prevents ER-positive and ER-negative mammary tumors in p53-null mammary gland mice. Cancer Prev Res 2012;5:1195–202.
28. Zhang M, Behbod F, Atkinson RL, Landis MD, Kittrell F, Edwards D, et al. Identification of tumor-initiating cells in a p53-null mouse model of breast cancer. Cancer Res 2008;68:4674–82.
29. Vadakkan TJ, Landua JD, Bu W, Wei W, Li F, Wong ST, et al. Wnt-responsive cancer stem cells are located close to distorted blood vessels and not in hypoxic regions in a p53-null mouse model of human breast cancer. Stem Cells Transl Med 2014;3:857–66.
30. Nguyen DH, Oketch-Rabah HA, Illa-Bochaca I, Geyer FC, Reis-Filho JS, Mao JH, et al. Radiation acts on the microenvironment to affect breast carcinogenesis by distinct mechanisms that decrease cancer latency and affect tumor type. Cancer Cell 2011;19:640–51.
31. Nguyen DH, Fredlund E, Zhao W, Perou CM, Balmain A, Mao J-H, et al. Murine microenvironment metaprofiles associate with human cancer etiology and intrinsic subtypes. Clin Cancer Res 2013;19:1353–62.
32. Harvey JM, Clark GM, Osborne CK, Allred DC. Estrogen receptor status by immunohistochemistry is superior to the ligand-binding assay for predicting response to adjuvant endocrine therapy in breast cancer. J Clin Oncol 1999;17:1474–81.
33. Carvalho BS, Irizarry RA. A framework for oligonucleotide microarray preprocessing. Bioinformatics 2010;26:2363–7.
34. Pavlidis P, Noble W. Analysis of strain and regional variation in gene expression in mouse brain. Genome Biol 2001;2:RESEARCH0042.
35. Rakha EA, Ellis IO. Triple-negative/basal-like breast cancer: review. Pathology 2009;41:40–7.
36. Tang J, Fernandez-Garcia I, Vijayakumar S, Martinez-Ruiz H, Illa-Bochaca I, Nguyen DH, et al. Irradiation of juvenile, but not adult, mammary gland increases stem cell self-renewal and estrogen receptor negative tumors. Stem Cells 2013;32:649–61.
37. Visvader JE. Cells of origin in cancer. Nature 2011;469:314–22.
38. Santagata S, Thakkar A, Ergonul A, Wang B, Woo T, Hu R, et al. Taxonomy of breast cancer based on normal cell phenotype predicts outcome. J Clin Invest 2014;124:859–70.
39. Lim E, Wu D, Pal B, Bouras T, Asselin-Labat ML, Vaillant F, et al. Transcriptome analyses of mouse and human mammary cell subpopulations reveal multiple conserved genes and pathways. Breast Cancer Res 2010;12:R21.
40. Ringnér M, Fredlund E, Häkkinen J, Borg Å, Staaf J. GOBO: gene expression-based outcome for breast cancer online. PLoS ONE 2011;6:e17911.
41. Reedijk M, Odorcic S, Chang L, Zhang H, Miller N, McCready DR, et al. High-level coexpression of JAG1 and NOTCH1 is observed in human breast cancer and is associated with poor overall survival. Cancer Res 2005;65:8530–7.
42. Bouras T, Pal B, Vaillant F, Harburg G, Asselin-Labat M-L, Oakes SR, et al. Notch signaling regulates mammary stem cell function and luminal cell-fate commitment. Cell Stem Cell 2008;3:429–41.
43. Costes S, Streuli CH, Barcellos-Hoff MH. Quantitative image analysis of laminin immunoreactivity in skin basement membrane irradiated with 1 GeV/nucleon iron particles. Radiat Res 2000;154:389–97.
44. Lorimore SA, Coates PJ, Wright EG. Radiation-induced genomic instability and bystander effects: inter-related nontargeted effects of exposure to ionizing radiation. Oncogene 2003;22:7058–69.
45. NAS/NRC. Health risks from exposure to low levels of ionizing radiation: phase 2. Washington, D.C.: National Academy Press; 2006.
46. Fornace AJJ, Amundson SA, Bittner M, Myers TG, Meltzer P, Weinsten JN, et al. The complexity of radiation stress responses: analysis by informatics and functional genomics approaches. Gene Expr 1999;7:387–400.
47. Tsai KK, Chuang EY, Little JB, Yuan ZM. Cellular mechanisms for low-dose ionizing radiation-induced perturbation of the breast tissue microenvironment. Cancer Res 2005;65:6734–44.
48. Andarawewa KL, Costes SV, Fernandez-Garcia I, Chou WS, Ravani SA, Park H, et al. Radiation dose and quality dependence of epithelial to mesenchymal transition (EMT) mediated by transforming growth factor β. Int J Rad Onc Biol Phys 2011;79:1523–31.

Cancer Research
The Journal of Cancer Research (1916–1930) | The American Journal of Cancer (1931–1940)

AACR American Association for Cancer Research

Densely Ionizing Radiation Acts via the Microenvironment to Promote Aggressive *Trp53*-Null Mammary Carcinomas

Irineu Illa-Bochaca, Haoxu Ouyang, Jonathan Tang, et al.

Cancer Res Published OnlineFirst October 10, 2014.